B cell antigen extraction is regulated by physical properties of antigen-presenting cells

Katelyn M. Spillane[1,2] and Pavel Tolar[1,2]

[1]Immune Receptor Activation Laboratory, The Francis Crick Institute, London NW1 1AT, England, UK
[2]Division of Immunology and Inflammation, Imperial College London, London SW7 2AZ, England, UK

Antibody production and affinity maturation are driven by B cell extraction and internalization of antigen from immune synapses. However, the extraction mechanism remains poorly understood. Here we develop DNA-based nanosensors to interrogate two previously proposed mechanisms, enzymatic liberation and mechanical force. Using antigens presented by either artificial substrates or live cells, we show that B cells primarily use force-dependent extraction and resort to enzymatic liberation only if mechanical forces fail to retrieve antigen. The use of mechanical forces renders antigen extraction sensitive to the physical properties of the presenting cells. We show that follicular dendritic cells are stiff cells that promote strong B cell pulling forces and stringent affinity discrimination. In contrast, dendritic cells are soft and promote acquisition of low-affinity antigens through low forces. Thus, the mechanical properties of B cell synapses regulate antigen extraction, suggesting that distinct properties of presenting cells support different stages of B cell responses.

Introduction

Production of high-affinity antibodies against pathogens is an effective mechanism of protection against a wide range of infections. Antibody responses are initiated when naive B cells bind foreign antigens on the surfaces of several types of cells, such as subcapsular sinus macrophages (Carrasco and Batista, 2007; Junt et al., 2007; Phan et al., 2007), dendritic cells (DCs; Qi et al., 2006; Gonzalez et al., 2010), and follicular dendritic cells (FDCs; Suzuki et al., 2009). These cells retain and display unprocessed antigen on their surfaces, and we refer to them here as antigen-presenting cells (APCs). The encounter of B cells with antigen on the APCs induces B cell receptor (BCR) signaling, BCR–antigen microcluster formation, contraction of microclusters into a mature immune synapse, and antigen internalization. The internalized antigens are processed, loaded onto major histocompatibility complex class II (MHCII) molecules, and presented to helper T cells (Batista et al., 2001; Fleire et al., 2006; Natkanski et al., 2013). After T cell engagement, B cells can enter the germinal center (GC), which is required for the development of affinity-matured plasma cells and memory B cells (Victora and Nussenzweig, 2012). The likelihood that a B cell will enter and expand within the GC depends on the affinity of the BCR for antigen and is limited by T cell help (Shih et al., 2002; Victora et al., 2010; Schwickert et al., 2011), suggesting that the quality of BCR–antigen binding regulates the efficiency of antigen internalization. The mechanisms that link antigen binding strength to antigen extraction and internalization remain, however, poorly understood.

When presenting antigens to B cells, APCs use a variety of receptors including complement receptors, Fc receptors, and C-type lectins (Fang et al., 1998; Bergtold et al., 2005). However, it remains unclear how B cells extract antigen from these receptors. In two early studies, Batista and Neuberger showed that B cells can acquire antigen tethered to a surface and proposed that extraction occurs via mechanical forces (Batista and Neuberger, 2000; Batista et al., 2001). Direct evidence supporting this hypothesis was provided recently, in studies demonstrating that B cells physically pull on synaptic antigen through the BCR and deform flexible membrane substrates to promote antigen internalization (Natkanski et al., 2013; Nowosad et al., 2016). Mechanical forces provide an added benefit of allowing B cells to test the strength of synaptic antigen binding by applying tension to the BCR–antigen bond, resulting in affinity-dependent extraction and internalization of BCR microclusters (Tolar and Spillane, 2014).

An alternative mechanism of B cell antigen extraction based on enzymatic degradation of antigen in the synapse has also been proposed (Yuseff et al., 2011; Reversat et al., 2015). This mechanism is based on the observation that B cells polarize the microtubule-organizing center toward the synapse, leading to recruitment of lysosomal-associated membrane protein 1 (LAMP-1)–positive lysosomes to the plasma membrane. This

Correspondence to Pavel Tolar: pavel.tolar@crick.ac.uk

Abbreviations used: APC, antigen-presenting cell; BCR, B cell receptor; DC, dendritic cell; FDC, follicular dendritic cell; GC, germinal center; LAMP, lysosomal-associated membrane protein; MHC, major histocompatibility complex; PEG, polyethylene glycol; PLB, planar lipid bilayer; PMS, plasma membrane sheet; SUV, small unilamellar vesicle.

© 2017 Spillane and Tolar This article is distributed under the terms of an Attribution–Noncommercial–Share Alike–No Mirror Sites license for the first six months after the publication date (see http://www.rupress.org/terms/). After six months it is available under a Creative Commons License(Attribution–Noncommercial–Share Alike 4.0 International license, as described at https://creativecommons.org/licenses/by-nc-sa/4.0/).

The Rockefeller University Press $30.00
J. Cell Biol. Vol. 216 No. 1 217–230
https://doi.org/10.1083/jcb.201607064

THE JOURNAL OF CELL BIOLOGY

Downloaded from http://rupress.org/jcb/article-pdf/216/1/217/1373975/jcb_201607064.pdf by The Francis Crick Institute user on 20 October 2020

recruitment is followed by extracellular release of lysosomal proteases that liberate antigen from the presenting surface before internalization.

It is currently not clear whether mechanical forces and enzymatic degradation occur at the same time and potentiate each other in antigen extraction, or whether B cells use them in different situations. In addition, because all previous experiments were performed using artificial antigen-presenting substrates, it is not known which mechanism of B cell antigen extraction is the most relevant to interactions with live APCs and how it may influence different stages of B cell responses.

Here we developed new in situ, DNA-based molecular sensors that distinguish between mechanisms of B cell antigen extraction from both artificial substrates and live APCs. We show that the mechanism of antigen extraction depends on the physical properties of the presenting substrate. B cells used primarily force-based extraction, although they did resort to enzymatic degradation when mechanical antigen extraction was not possible. Importantly, force-based extraction was used exclusively to extract antigen from live APCs.

Using DNA-based tension sensors, we also show that the efficiency of force-based extraction depends on the stiffness of the substrate, antigen tethering strength, and BCR affinity. Stiff substrates in particular promoted application of strong forces by the B cells and improved affinity discrimination. We found that FDCs were stiffer than DCs and, like stiff artificial substrates, promoted generation of strong forces and stringent antigen affinity discrimination by B cells. In contrast, the flexible membranes of DCs promoted extraction of low-affinity antigen by weak pulling forces. Collectively, our data reveal that mechanical cues received in the immune synapse play a role in regulating B cell responses.

Results

DNA-based molecular sensors report B cell antigen degradation with high sensitivity

We designed a DNA-based fluorescent sensor to report intracellular and extracellular enzymatic antigen degradation for use in live or fixed cells. The sensor consists of a 25-bp DNA duplex with a fluorophore and quencher in close proximity at one end and a biotin for coupling to antigen on the opposite end (Fig. 1 A and Fig. S1 A). We selected Atto647N and Iowa Black RQ from nine fluorophore-quencher pairs, achieving a quenching efficiency of >98% over a pH range of 4–7.4 (Fig. S1, B and C). Stability at acidic pH was important to ensure that any change in fluorescence signal was caused by sensor degradation and not low pH in the endosomes. In solution, there was a 200-fold difference in fluorescence signal between the quenched and unquenched sensors at pH 4.0 (Fig. S1 D).

To demonstrate that this sensor reports intracellular degradation, we bound soluble antigen (anti-Igκ) tethered to the degradation sensor to naive B cells and incubated the cells at either 4°C or 37°C. Cells that were allowed to internalize the antigen at 37°C showed a 20-fold increase in Atto647N fluorescence signal over those incubated at 4°C by flow cytometry (Fig. 1, B and C). We verified that this increase in fluorescence was caused by degradation of the sensor by stabilizing the sensor against nuclease degradation using 2′-OMe phosphorothioate–modified DNA. We found that the modified sensor showed minimal increase in Atto647N fluorescence after internalization by B cells (Fig. 1, B and C).

Because the DNA-based sensors report nuclease-mediated degradation, and not protein antigen processing directly, we next sought to determine whether degradation of the DNA sensor occurs in the same intracellular compartments as degradation of protein antigens. We incubated B cells with soluble antigens (anti-Igκ) bound to both the DNA degradation sensor and DQ Green BSA (DQ-BSA), a fluorescent reporter of proteolysis. After incubating the cells for 0–20 min at 37°C, we measured colocalization of internalized antigen, degraded DNA sensor, and degraded DQ-BSA (Fig. 1 D). We observed that DNA and protein degradation always occurred together in the same antigen-containing compartments, indicating that the DNA sensor accurately reported B cell antigen degradation. Degradation of both the DNA sensor and DQ-BSA increased over time, although the DNA sensor was markedly more sensitive to degradation than DQ-BSA as shown by a larger change in fluorescence intensity upon unquenching (Fig. 1, D and E). We also observed rapid association of antigen-containing endosomes with LAMP-1 (Fig. S2, A and B) followed by a gradual increase in degradation of the colocalized DNA sensor (Fig. S2, A and C). Thus, DNA and protein degradation occurred in the same LAMP-1$^+$ lysosomal compartments.

To observe whether B cells degrade membrane-presented antigen extracellularly, we presented DNA degradation sensor–conjugated antigen (Cy3-labeled NIP_{10}) to B1-8 B cells on planar lipid bilayers (PLBs) and plasma membrane sheets (PMSs), two membrane substrates that have been used to mimic APCs (Fleire et al., 2006; Natkanski et al., 2013). We observed increased DNA sensor fluorescence in B cell contacts formed with PLBs, suggesting antigen degradation in the extracellular space of the synapse (Fig. 1, F and G). The sensor was not degraded in synapses formed on PMSs, although it was degraded once internalized. Importantly, an increase in fluorescence was not observed for the nuclease-resistant DNA sensor. Together, these results suggest that different antigen-presenting substrates instruct B cells to manipulate antigen using different mechanisms.

B cells use different antigen extraction mechanisms depending on the physical properties of the antigen-presenting substrate

To determine the contribution of degradation- and force-based mechanisms to extraction of tethered antigen, we developed a DNA-based sensor that provides a color-coded readout of enzymatic versus mechanical antigen extraction (Fig. 2 A). The mechanism sensor comprises two 24-bp handles connected by a single nucleotide. The top handle is covalently bound to antigen (NIP_{10}) labeled with Atto550 fluorophores, and the bottom handle is modified with an Atto647N fluorophore and a biotin for tethering to a substrate. If the B cell degrades antigen in the synapse to promote extraction before internalization, then the DNA is cleaved and only the Atto550-labeled antigen is extracted. However, if the B cell extracts antigen through mechanical force, then the DNA remains intact and both the Atto550 and Atto647N fluorophores are internalized into the same endosomal compartments.

We investigated whether the physical characteristics of the antigen-presenting substrate influence B cell behavior by presenting the mechanism sensor on three artificial substrates that differ in stiffness and mobility: glass modified with polyethylene glycol (PEG; stiff and immobile), PLBs (stiff and highly mobile), and PMSs (flexible and partly mobile). Antigen

Downloaded from http://rupress.org/jcb/article-pdf/216/1/217/1373975/jcb_201607064.pdf by The Francis Crick Institute user on 20 October 2020

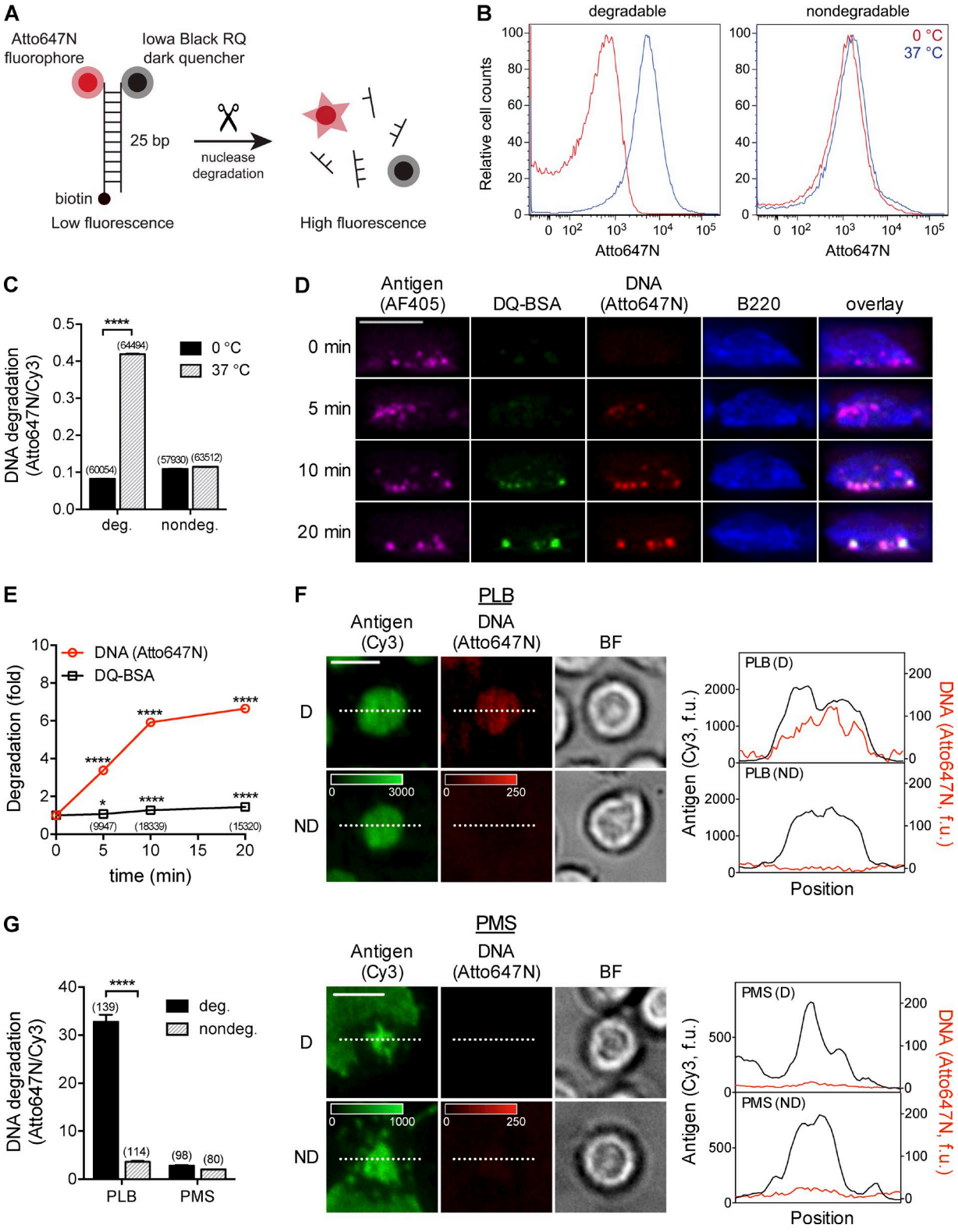


Figure 1. **Visualizing intracellular and extracellular B cell antigen degradation using DNA-based molecular sensors.** (A) Schematic of the DNA degradation sensor. (B) Flow cytometry histograms showing Atto647N fluorescence intensity before (0°C) and after (37°C) naive B cell internalization of soluble antigen (Cy3–anti-Igκ) tethered to the degradable (deg.) and nondegradable (nondeg.) DNA sensors. (C) Degradation of the DNA sensor, quantified as the DNA Atto647N fluorescence intensity normalized to the antigen Cy3 fluorescence intensity from flow cytometry (mean and SEM; cell numbers are shown in parentheses above each bar). Data are from one experiment representative of two independent experiments. (D) Side-view reconstructions of B cells internalizing soluble antigen (AF405–anti-Igκ) simultaneously tethered to DQ-BSA and the DNA degradation sensor. Time-dependent colocalization of the degraded DQ-BSA and the degraded DNA sensor signal (Atto647N) are shown. Bar, 5 µm. (E) Time-dependent degradation of the DNA sensor and DQ-BSA in antigen-containing clusters, showing fold change of DNA or DQ-BSA fluorescence intensity normalized to the antigen fluorescence intensity. Data are mean and SEM for the cluster numbers shown in parentheses below the markers (the SEM error bars are smaller than the size of the markers).

Downloaded from http://rupress.org/jcb/article-pdf/216/1/217/1373975/jcb_201607064.pdf by The Francis Crick Institute user on 20 October 2020

tethered to glass via PEG is immobilized on the surface, whereas PLB and PMS are both membrane substrates that exhibit similar levels of lipid and antigen mobility (Natkanski et al., 2013). However, PLBs and PMSs have different viscoelastic properties that impact the ability of B cells to extract and internalize antigen. PLBs are separated from the supporting glass surface by only a 1- to 2-nm water layer (Castellana and Cremer, 2006), allowing strong adhesion between the lipids and glass support that promotes strong resistance to membrane deformation (Lipowsky and Seifert, 1991). In contrast, PMSs are suspended ∼10 nm from the glass surface because of the presence of transmembrane proteins, resulting in poor adhesion to the underlying glass support and high PMS viscoelasticity (Natkanski et al., 2013). Tethering of sensors to PEG and PLB was achieved via a streptavidin linker to singly biotinylated PEG and lipids, creating a homogeneous distribution of sensors on these surfaces. Sensors were coupled to PMS through streptavidin linked to biotinylated Annexin V, which caused sensors to be distributed on the surface in small clusters.

Images of fixed B1-8 B cells show clear differences in synapse formation on the three substrates (Fig. 2 B). On PEG, the sensor was homogeneously distributed throughout the synapse except for a dark ring around the outer edge that indicates sensor extraction near the B cell lamellipodia. On the mobile PLBs and PMSs, B cells gathered the sensors into the center of the contact area to form a mature synapse. On PMSs, we also observed a significant loss of sensor fluorescence in the area surrounding the synapse, suggesting that B cells extracted a large amount of antigen from this region.

Z-stack images, side-view reconstructions of individual B cells, and image quantification showed that B cells internalized antigen from each substrate, although by different mechanisms and with different efficiencies (Fig. 2 C). B cells internalized both fluorophores of the mechanism sensor when it was tethered to PEG and PMSs, suggesting primarily force-mediated extraction (Fig. 2, C and D). When the sensor was presented on PLBs, B cells internalized only Atto550, but not Atto647N (Fig. 2, C and D), indicating extraction through enzymatic degradation. This result is in agreement with our observation that B cells degraded DNA in synapses formed on this substrate (Fig. 1, F and G). Quantification of total antigen extraction showed that B cells acquired the most antigen from PMSs and the least from PLBs (Fig. 2 E), indicating that mechanical force was the more efficient antigen extraction mechanism.

In B cells extracting the mechanism sensor from PEG and PMS, all endosomes contained both Atto647N and Atto550. However, there was a small difference in the endosomal Atto647N/Atto550 fluorescence intensity ratios between B cells on PEG and PMSs (Fig. 2 D). Although we cannot exclude the possibility that this was caused by a small amount of degradation in the synapse alongside mechanical antigen extraction from PEG, we attribute the ratio difference to changes in fluorescence resonance energy transfer between the Atto550 and Atto647N fluorophores, which was affected by the sensor density on each substrate (Fig. S3 A) and the degradation in intracellular compartments (Fig. S3 B).

B cells acquired the streptavidin tether from PMSs but not PEG, suggesting different rupture sites from the two substrates (Fig. 2, C and F). This is consistent with the flexibility of PMSs, which makes it possible for B cells to pinch off a portion of the membrane during mechanical extraction, resulting in internalization of streptavidin in addition to the sensor. B cells cannot invaginate the stiff PEG substrate, however, so rupture instead occurs between the biotin on the sensor and streptavidin on the substrate. Extraction of antigen from biotin–streptavidin tethers has been observed before (Batista and Neuberger, 2000) and is possibly enabled by a cumulative effect of sustained lateral forces applied to the biotin–streptavidin bond through multivalent BCR–antigen interactions. Collectively, these results suggest that the mechanism and efficiency of B cell antigen extraction depend on the physical properties of antigen presentation.

Mechanical force is the dominant B cell antigen extraction mechanism

We next sought to understand whether B cells liberated antigen enzymatically from PLBs because of the intrinsic mechanical properties of this substrate, or because mechanical extraction was not possible. The lack of mechanical extraction could be caused by the combination of strong biotin–streptavidin tethering and weak forces generated by B cells on PLBs as a result of lateral antigen slippage (Nowosad et al., 2016). To investigate this, we designed a DNA-based tension sensor that is thermodynamically stable but releases the antigen if the B cell applies mechanical forces higher than a low rupture force of ∼12 pN to the BCR–antigen bond (Fig. 3 A). The sensor consists of 24-bp upper and lower handles connected by a 20-bp duplex in the unzipping configuration (Krautbauer et al., 2003; Wang and Ha, 2013). The upper handle is covalently bound to antigen (NIP_{10}) and labeled with an Atto647N fluorophore, and the lower handle is labeled with Atto550 and contains two biotins for tethering to a substrate. We found that B1-8 B cells were able to unzip the tension sensor attached to the PLBs and internalize the upper handle while leaving the lower handle tethered to the PLB (Fig. 3 B). This suggests that B cells can extract antigen from PLBs by mechanical force if the tethering strength is sufficiently low.

To determine whether B cells use both mechanical and enzymatic extraction mechanisms cooperatively to acquire antigen, or whether B cells preferentially use one extraction mechanism over the other, we presented the mechanism sensor doped with 0.1% of the tension sensor on PLBs to B1-8 B cells. Both sensors were conjugated to the same antigen (NIP_{10}), and the upper handle of the tension sensor was labeled with Atto488 to distinguish it spectrally from the Atto550 and Atto647N fluorophores on the mechanism sensor. We observed that enzymatic

Data are from one experiment representative of two independent experiments. Statistics refer to fold change increase higher than DNA or DQ-BSA background fluorescence level at 0 min. (F, left) Total internal reflection fluorescence images of synapses formed by B1-8 B cells on PLBs or PMSs loaded with antigen (Cy3-NIP_{10}) tethered to a degradable (D) or nondegradable (ND) DNA sensor. BF, bright field. Bars, 5 µm. Images showing antigen fluorescence intensities were scaled differently for PLB and PMS substrates, as indicated by the calibration bars. (F, right) Linescans showing the antigen and DNA fluorescence intensities along the dotted lines indicated in the images. f.u., fluorescence units. (G) Quantification of DNA sensor degradation in synapses formed on PLBs and PMSs, calculated as the DNA sensor fluorescence intensity normalized to the antigen fluorescence intensity in the synapse (mean and SEM; cell numbers are shown in parentheses above each bar). Data are from one experiment representative of two independent experiments. *, $P < 0.05$; ****, $P < 0.0001$ (unpaired *t* tests).

Downloaded from http://rupress.org/jcb/article-pdf/216/1/217/1373975/jcb_201607064.pdf by The Francis Crick Institute user on 20 October 2020

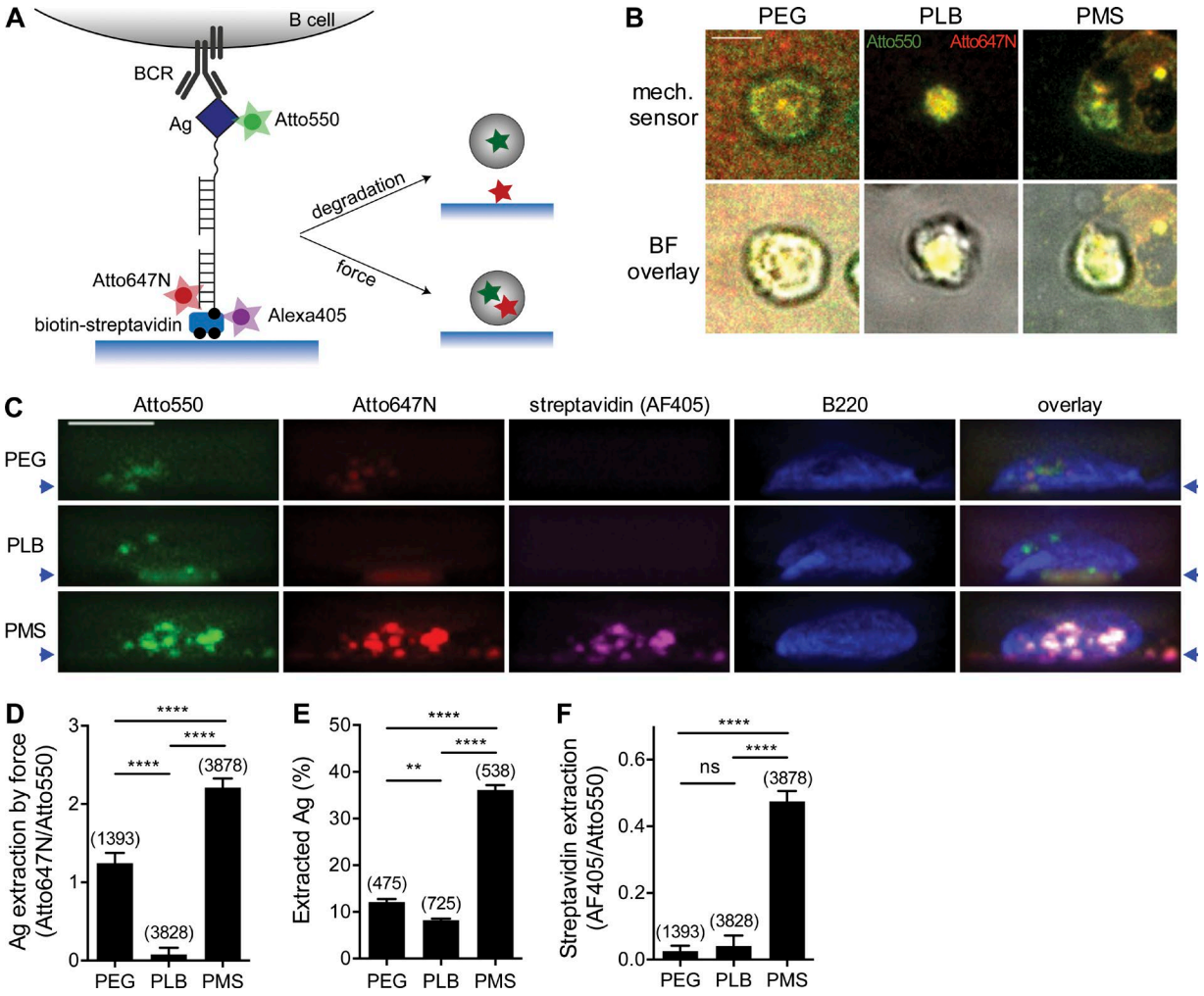


Figure 2. **B cells change the antigen extraction mechanism depending on the physical properties of antigen-presenting substrates.** (A) Schematic of the mechanism sensor. (B) Representative total internal reflection fluorescence images of the contact areas between B1-8 B cells and the mechanism (mech.) sensor (presenting NIP_{10} antigen) tethered to PEG-coated glass, PLB, or PMS substrates. BF, bright field. (C) Side-view reconstructions of B220-stained B1-8 B cells that have extracted the mechanism sensor from each substrate. Note that the substrate surfaces are not clearly visible because of the deconvolution procedure for the image display, which removes smooth, unclustered signal from the images. Therefore, we included blue arrows to mark the positions of the substrates. (D) Quantification of Atto647N/Atto550 fluorescence intensity ratios in antigen (Ag) clusters internalized from PEG, PLB, and PMS substrates. (E) Quantification of total B cell antigen extraction (Atto550 fluorescence intensity) from each substrate (mean and SEM; cell numbers are shown in parentheses above each bar). (F) Quantification of streptavidin extracted, calculated as antigen cluster AF405/Atto550 intensity ratios. Error bars in D and F represent mean and SEM for the cluster numbers shown in parentheses above each bar. Data are from one experiment representative of three independent experiments. **, $P < 0.01$; ****, $P < 0.0001$ (nonparametric *t* tests). Bars, 5 µm.

extraction of antigen was almost completely eliminated when B cells could extract a small amount of antigen through mechanical force (Fig. 3 C), suggesting that mechanical extraction of antigen precedes enzymatic liberation. Further, these results indicate that B cells do not use enzymatic and mechanical extraction mechanisms cooperatively, but rather that B cells preferentially acquire antigen through mechanical force.

To understand how B cells could extract antigen mechanically from the tension sensor while simultaneously engaging but not extracting antigen from the mechanism sensor, we imaged B cells interacting with PLBs containing a 1:1 mixture of the sensors. The sensors always colocalized in the early BCR microclusters and also in 75% of mature B cell synapses (Fig. S4 A), although we did observe some spatial separation in the mature synapses for the remaining population (Fig. S4 B). Spatial segregation of sensors in the synapse did not correlate with antigen internalization, suggesting that it was not obligatory for force-mediated extraction (Fig. S4 C). Because the unzipping geometry of the tension sensor buffers the force across the BCR–antigen bond, and the shearing geometry of the mechanism sensor enhances the load on the bond, it is likely that B cells were able to extract antigen mechanically from the tension sensor while rupturing BCR bonds to the mechanism sensor.

Interestingly, there was no difference in LAMP-1$^+$ lysosome polarization when B cells were stimulated by the mechanism or tension sensors, or a 1:1 sensor mixture, on PLBs (Fig. 3 D). However, lysosomes were polarized in a small population of B cells that interacted with, but did not extract, antigen conjugated to the tension sensor (Fig. 3 E). These data suggest that B cell antigen extraction, by either enzymatic liberation or mechanical force, halts recruitment and accumulation of lysosomes in the synapse.

To examine lysosome polarization in more detail, we tracked the movement of LAMP-1$^+$ lysosomes after engagement

Downloaded from http://rupress.org/jcb/article-pdf/216/1/217/1373975/jcb_201607064.pdf by The Francis Crick Institute user on 20 October 2020

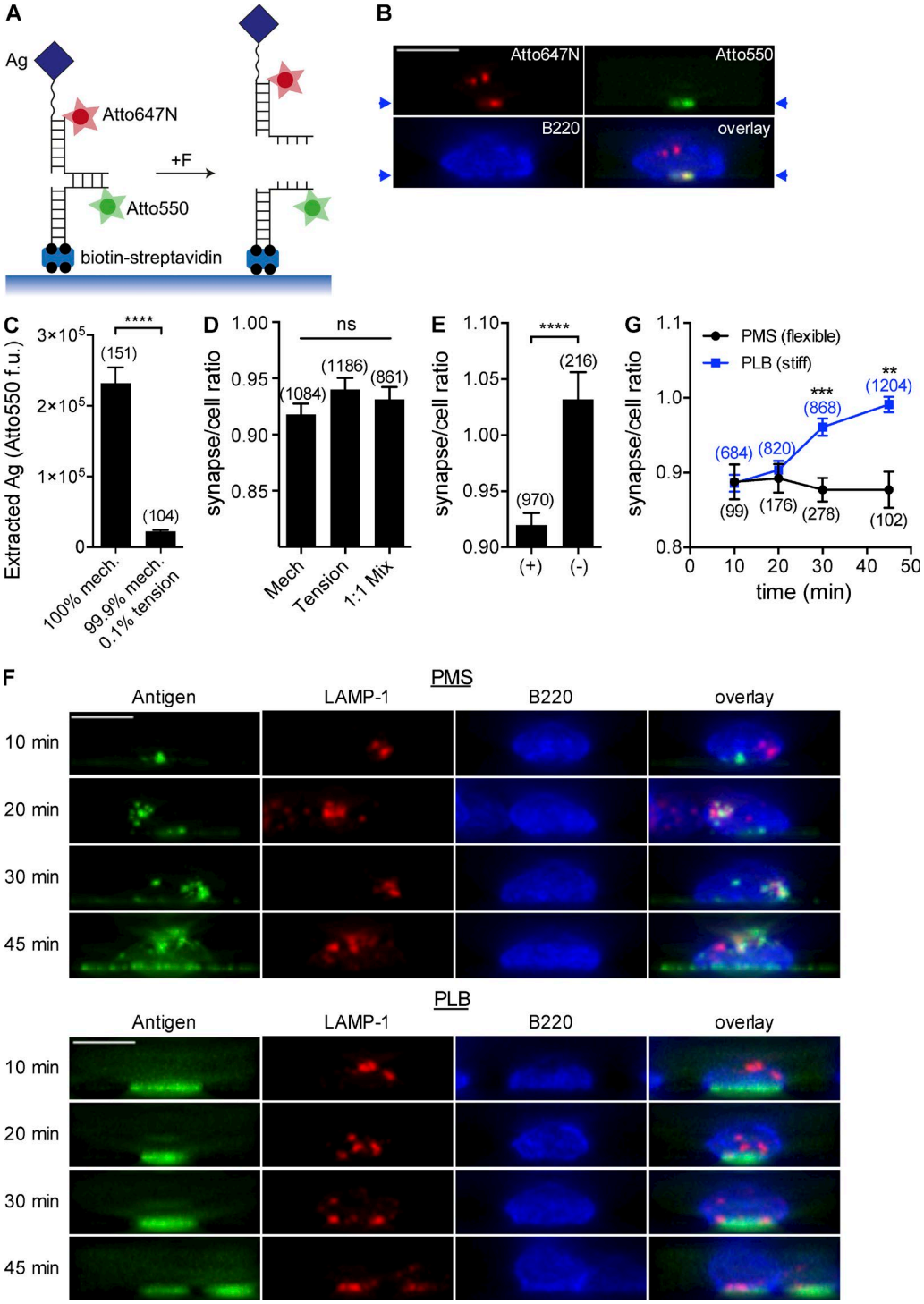


Figure 3. **Mechanical force is the dominant antigen extraction mechanism.** (A) Schematic of the DNA-based tension sensor. Ag, antigen. (B) Side-view reconstruction of a B cell that has unfolded the tension sensor to extract the antigen (NIP_{10}) and upper handle (Atto647N) from a PLB, leaving the lower handle (Atto550) of the sensor behind. The blue arrows indicate the position of the substrate. Bar, 5 µm (C) Antigen (NIP_{10}) extracted through enzymatic degradation when 0% or 0.1% of the antigen is attached to the tension sensor. Error bars represent mean Atto550 fluorescence intensity in extracted antigen clusters and SEM for the cell numbers shown in parentheses above each bar. Data are from one experiment representative of two independent experiments. f.u., fluorescence units. (D) LAMP-1$^+$ vesicle recruitment to the plasma membrane calculated as the ratio of synaptic to total cell LAMP-1 intensity for B1-8 B cells binding NIP_{10} antigen tethered to the mechanism (mech) sensor, tension sensor, or a 1:1 sensor mixture on PLBs. (E) LAMP-1$^+$ vesicle recruitment to the plasma membrane for B1-8 B cells that either did (+) or did not (–) internalize NIP_{10} antigen from the tension sensor on PLBs. In D and E, data are mean and SEM for the cell numbers indicated in parentheses above each bar, and are from one experiment representative of two independent experiments. (F) Side-view reconstructions showing antigen and LAMP-1$^+$ vesicles in naive B cells binding antigen (anti-Igκ) anchored directly via biotin–streptavidin–biotin linkers to PMSs or PLBs. Bars, 5 µm. (G) Time course of LAMP-1$^+$ vesicle recruitment to the plasma membrane on PLBs and PMSs (mean and SEM; cell numbers are shown in parentheses adjacent to the markers). Data are from one experiment representative of two independent experiments. ****, $P < 0.0001$; ***, $P < 0.001$; **, $P < 0.01$ (unpaired *t* tests).

Downloaded from http://rupress.org/jcb/article-pdf/216/1/217/1373975/jcb_201607064.pdf by The Francis Crick Institute user on 20 October 2020

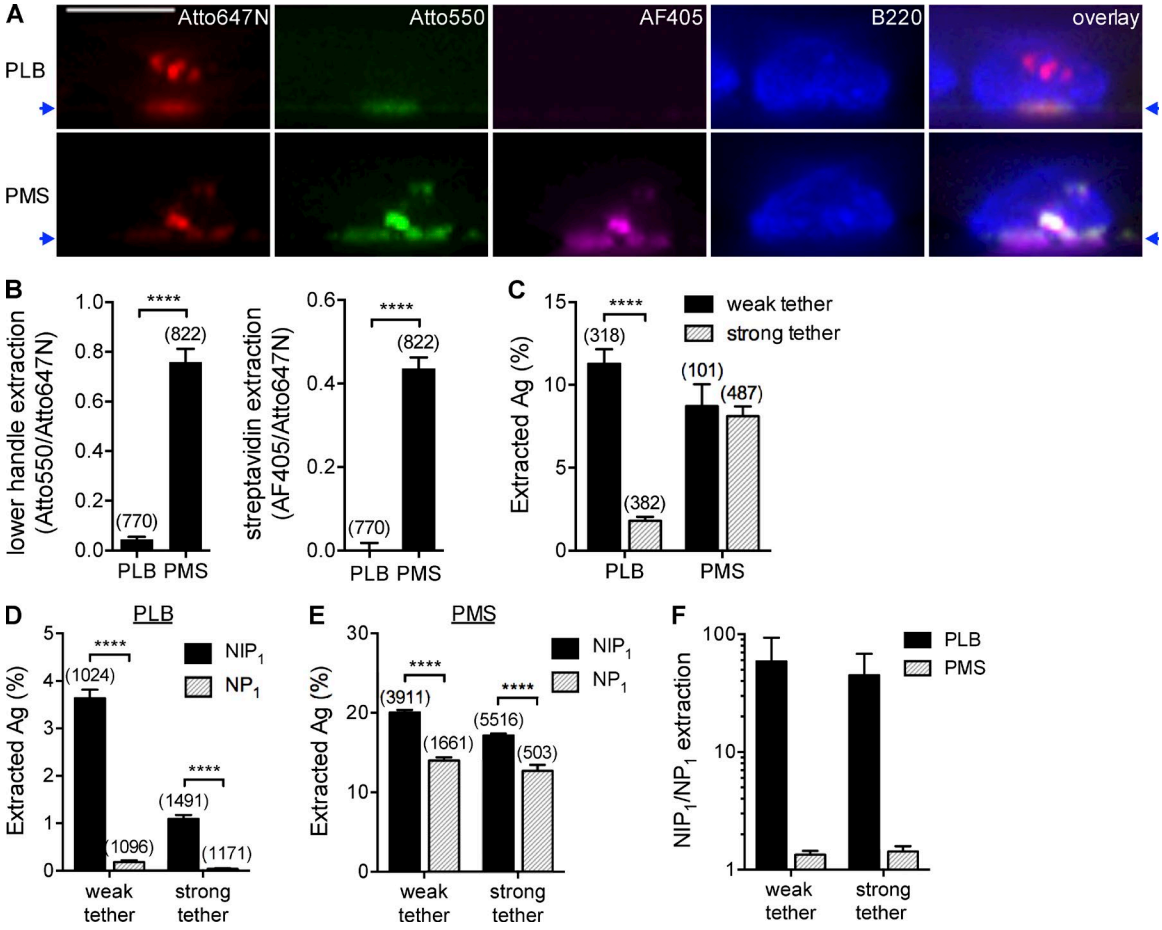


Figure 4. **Substrate flexibility, antigen tethering strength, and antigen affinity regulate B cell antigen extraction.** (A) Side-view reconstructions of B1-8 B cells that have extracted antigen (NIP_{10}) from the tension sensor on stiff (PLB) and flexible (PMS) substrates. (B) Extraction of the tension sensor's lower handle or streptavidin by B1-8 B cells from PLBs or PMSs. Data are mean fluorescence intensities in extracted antigen clusters (Atto550, lower handle; AF405, streptavidin) normalized to Atto647N fluorescence ± SEM. Cluster numbers are shown above the bars. (C) Extraction of NIP_{10} antigen (Ag) by B1-8 B cells from tension sensors providing a weak or strong tether from PLBs or PMSs. Graphs represent mean extracted antigen percent per cell and SEM. Data are from one experiment representative of three independent experiments. (D and E) Extraction of NIP_1 and NP_1 antigens by B1-8 B cells from weak and strong tethers from PLBs (D) or PMSs (E). Data are mean and SEM from one experiment representative of three independent experiments. (F) Ratio of NIP_1 to NP_1 antigens extracted by B1-8 B cells from weak and strong tethers from PLBs and PMSs. Data are mean and SEM from three experiments on each substrate. In C–E, cell numbers are shown in parentheses above each bar. ****, $P < 0.0001$ (unpaired *t* tests). Bar, 5 µm.

of B cells with antigen (anti-Igκ) that was tethered strongly to PLBs or PMSs through multiple biotin–streptavidin bonds. B cells readily extracted antigen from PMSs (Natkanski et al., 2013). Within 20 min, LAMP-1$^+$ lysosomes colocalized with antigen-containing endosomes, and they remained associated for the duration of our measurements (Fig. 3 F). In contrast, when antigen was presented on PLBs and therefore could not be extracted, we observed an accumulation of lysosomes in the synapse 20–45 min after initial antigen binding (Fig. 3, F and G). Collectively, these results suggest that successful acquisition of antigen prevents recruitment of lysosomes to the synapse by intracellular sequestering of lysosomes through endosomal fusion.

Membrane flexibility, antigen tethering strength, and antigen affinity regulate antigen extraction from immune synapses

To mechanically extract antigen from a membrane substrate, B cells need to rupture the antigen from its tether or bend the presenting membrane to pinch the antigen off. To understand how tethering strength and substrate flexibility affect mechanical antigen extraction, we quantified extraction of NIP_{10} by B1-8 B cells from the tension sensor presented on stiff (PLB) and flexible (PMS) membrane substrates. B cells extracted only the top handle of the sensor when it was tethered to PLBs, whereas they extracted the entire sensor along with streptavidin from PMSs (Fig. 4, A and B). This result suggests that B cells generated forces higher than the rupture threshold of the sensor during antigen extraction from the stiff substrate. In contrast, lower forces were sufficient to acquire antigen from the flexible substrate because the B cells could pinch the sensor and streptavidin linker from the PMS. We investigated the effect of antigen tethering strength in more detail by changing the GC content of the sensor duplex from 20% to 100%, thereby creating tension sensors that provided a weak (~12 pN) or strong (~20 pN) antigen tether (Krautbauer et al., 2003). We found that the tethering strength had no effect on antigen extraction from the flexible PMSs (Fig. 4 C). In contrast, increasing the antigen tethering strength significantly reduced the amount of antigen B cells acquired from the stiff PLBs.

These results suggest that mechanical antigen extraction involves a BCR–antigen–tether tug-of-war. Bond ruptures in this complex are expected to reflect the relative binding strength

Downloaded from http://rupress.org/jcb/article-pdf/216/1/217/1373975/jcb_201607064.pdf by The Francis Crick Institute user on 20 October 2020

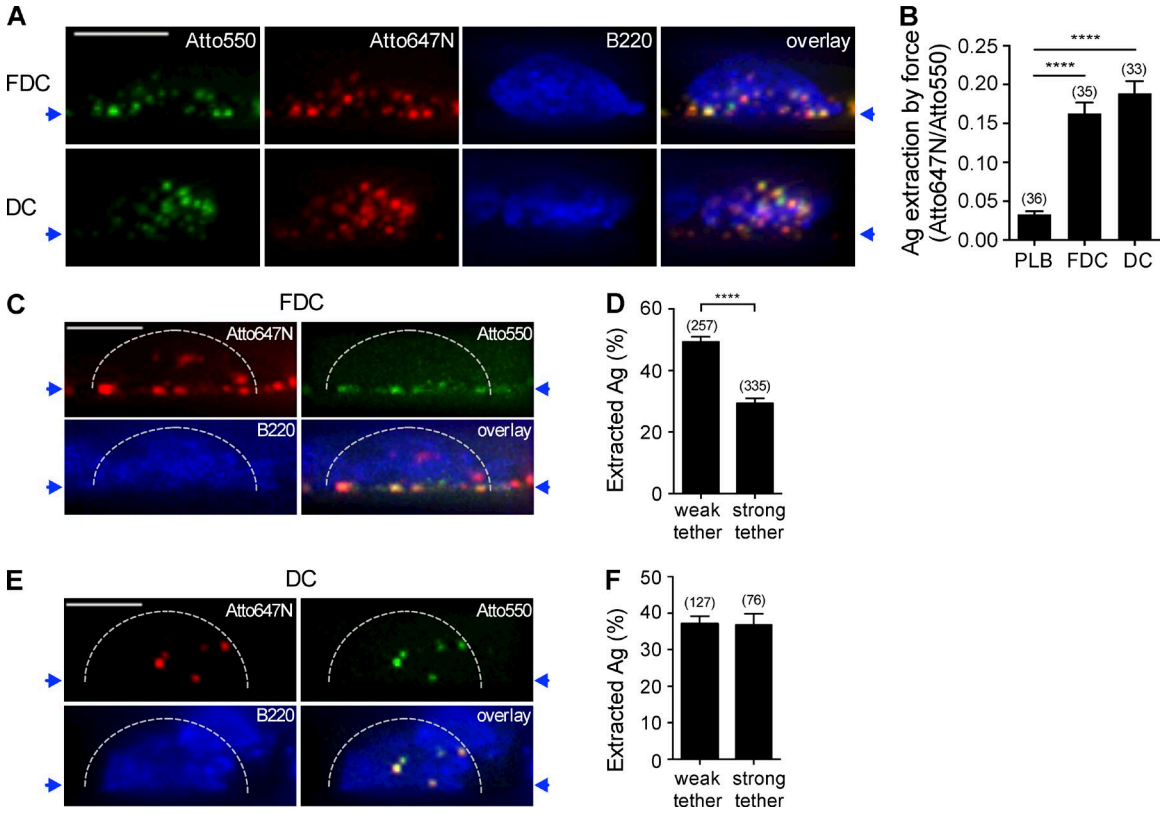


Figure 5. **B cells use mechanical force to extract antigen from live APCs.** (A) Side-view reconstructions of B1-8 B cells that have extracted the mechanism sensor from FDCs and DCs. Blue arrows indicate the position of the APC surface. (B) Quantification of antigen (Ag) cluster Atto647N/Atto550 intensity ratios extracted from PLBs, FDCs, and DCs. Data are mean and SEM from one experiment representative of three independent experiments. (C and E) Side-view reconstructions of B1-8 B cells that have extracted NIP_{10} antigen from the tension sensor on an FDC (C) or DC (E). Blue arrows indicate the position of the APC surface. B cells are outlined with dotted lines. (D and F) Extraction of NIP_{10} antigen from weak and strong tethers by B1-8 B cells from FDCs (D) or DCs (F). Data are mean and SEM from one experiment representative of two independent experiments. In B, D, and F, cell numbers are shown in parentheses above each bar. ****, $P < 0.0001$ (unpaired *t* tests). Bars, 5 µm.

of the BCR for antigen and the antigen for the tether, as well as the mechanical properties of the presenting membrane. We investigated the contributions of these different physical properties by measuring extraction of NIP_1 and NP_1 antigens tethered weakly and strongly to PLBs and PMSs (Fig. 4, D and E). NIP has a 10-fold higher 3D affinity for the B1-8 Fab fragment than NP does (Natkanski et al., 2013), making this system convenient for investigating the relative effects of BCR–antigen affinity and antigen tethering strength on B cell antigen extraction. We found that B1-8 B cells extracted significantly more NIP_1 than NP_1 regardless of tethering strength or substrate flexibility. On PLBs, B cells extracted significantly more of each antigen from the weak tether than the strong one, although a high antigen affinity could somewhat overcome the strong tether (Fig. 4 D). This finding supports the idea that antigen tethering strength and BCR–antigen affinity together regulate antigen extraction from stiff substrates (Batista and Neuberger, 2000). In contrast, on PMSs, the tethering strength had little effect on extraction (Fig. 4, C and E), suggesting that BCR–antigen affinity is the most important factor determining the efficiency of antigen extraction from flexible substrates. Further, although B cells extracted less antigen in total from PLBs than from PMSs, the ratio of total NIP_1 to NP_1 extracted was 20–30 times higher on PLBs (Fig. 4 F). Thus, affinity discrimination is more stringent on stiff substrates than flexible ones.

B cells use mechanical force to extract antigen from immune synapses with live APCs

The results presented so far show that the extraction mechanism, and the quality and quantity of extracted antigen, depend on the physical properties of the antigen-presenting substrate. To determine which extraction mechanism dominates under physiological conditions, we analyzed extraction of the mechanism sensor from live APCs. We chose FDCs and DCs as two important APCs that B cells encounter in vivo. We loaded the sensor onto APCs using streptavidin tethered to biotin- and complement-tagged immune complexes, binding to complement receptor 2 on FDCs or to Fc receptors on DCs, as observed in vivo (Fang et al., 1998; Bergtold et al., 2005). We observed complete colocalization of Atto550 and Atto647N in the B cell endosomes after sensor extraction from both APCs (Fig. 5 A). Further, the endosomal Atto647N/Atto550 fluorescence intensity ratio was significantly higher for FDCs and DCs compared with that of PLBs, indicating that B cells extract antigen from live APCs exclusively through mechanical force (Fig. 5 B). Notably, because B cells acquired the mechanism sensor intact, our data suggest that the FDCs and DCs did not degrade antigen in the synapse before extraction by B cells.

However, using the tension sensors, we determined that FDCs and DCs differ in their synaptic mechanical properties during antigen presentation. B cells extracted only the upper

Downloaded from http://rupress.org/jcb/article-pdf/216/1/217/1373975/jcb_201607064.pdf by The Francis Crick Institute user on 20 October 2020

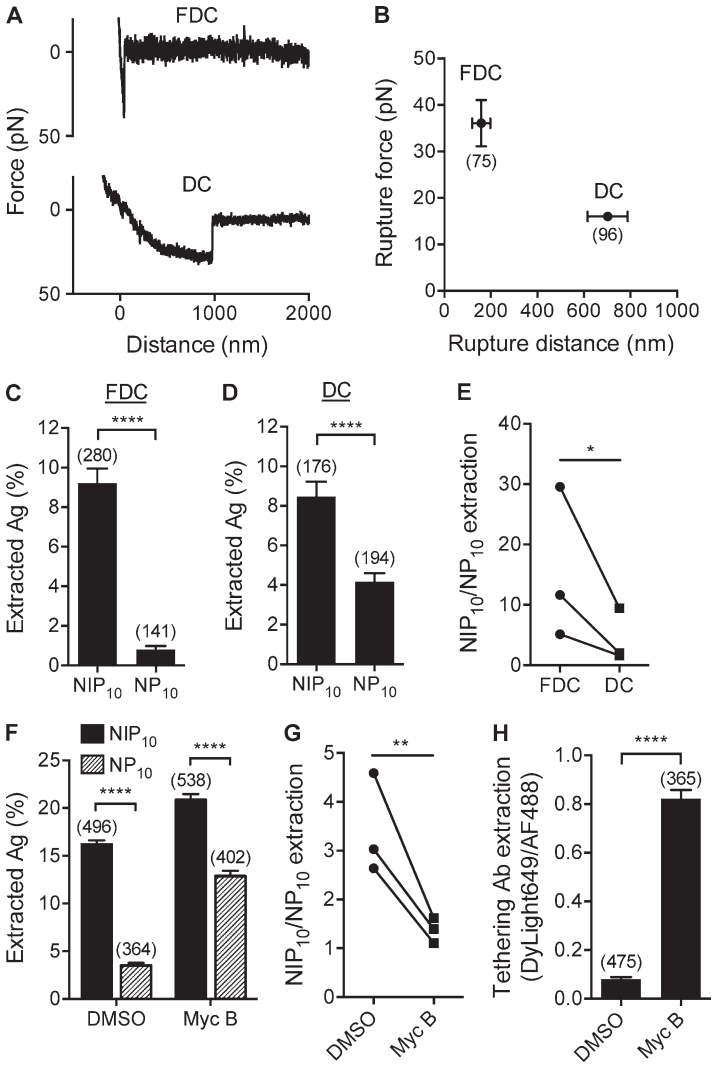


Figure 6. **Increased APC membrane tension promotes more stringent B cell antigen affinity discrimination.** (A) AFM spectroscopy retraction curves showing formation and rupture of membrane tethers from live FDCs or DCs. Speed of retraction was 2 µm/s. (B) Membrane tether rupture forces and distances measured by AFM spectroscopy (mean and SEM for the number of retraction curves shown in parentheses below each marker). (C and D) Extraction of NIP_{10} and NP_{10} antigens by B1-8 B cells from FDCs (C) and DCs (D). Data are mean and SEM for the cell numbers indicated in parentheses above each bar. Ag, antigen. ****, $P < 0.0001$ (unpaired *t* tests). Data are from one experiment representative of three independent experiments. (E) Ratios of NIP_{10} to NP_{10} antigen extracted from FDCs and DCs by B1-8 B cells from three independent experiments. *, $P < 0.05$ (paired *t* test). (F) Extraction of NIP_{10} and NP_{10} antigen by B1-8 B cells from FDCs treated with DMSO or 3 µM mycalolide B (Myc B). Bars represent mean extracted antigen per cell and SEM for the cell numbers indicated in parentheses above each bar. Data are from one experiment representative of three independent experiments. ****, $P < 0.0001$ (unpaired *t* test). (G) Ratios of NIP_{10} to NP_{10} antigen extracted from FDCs treated with DMSO or 3 µM Myc B by B1-8 B cells from three independent experiments. **, $P < 0.01$ (paired *t* test). (H) Co-extraction of the immune complex tethering antibody and protein antigen, calculated as the ratio of tethering antibody DyLight649 to NIP_{10} antigen AF488 fluorescence intensity in extracted antigen clusters. Data are mean and SEM for the cell numbers indicated in parentheses above each bar, from one experiment representative of three independent experiments. ****, $P < 0.0001$ (unpaired *t* test).

handle of the tension sensor from FDCs, leaving the lower handle bound to the FDC surface (Fig. 5 C). Further, B cells extracted significantly more weakly tethered antigen than strongly tethered antigen from FDCs (Fig. 5 D). These results suggest that FDCs enhance the strength of mechanical forces and promote force-dependent competition between BCR–antigen binding and antigen tethering strength, similarly to the stiff PLB substrates. In contrast, B cells extracted both the upper and lower handles of the tension sensor from DCs (Fig. 5 E), and the total antigen extracted was independent of the tethering strength (Fig. 5 F). Thus, DCs promote antigen extraction using lower mechanical forces and are therefore more similar to the flexible PMS substrates (Natkanski et al., 2013).

Physical properties of the APC regulate B cell antigen affinity discrimination

To characterize membrane flexibility of the two APCs directly, we used atomic force microscopy (AFM) and measured forces during binding of the AFM tip to the APC membranes and retraction until the rupture of the bond (Evans and Calderwood, 2007; Müller et al., 2009). On FDCs, forces during tip retraction increased rapidly to 30–40 pN and produced single-step bond ruptures 120–200 nm from the cell surface (Fig. 6, A and B), indicating high membrane stiffness. In contrast, on DCs, forces initially increased and then plateaued at ∼16 pN, with bonds rupturing 600–800 nm from the surface (Fig. 6, A and B). Thus, relative to FDCs, DCs have flexible plasma membranes.

We next investigated whether B cells could discriminate high- and low-affinity antigens during antigen extraction from FDCs and DCs. We observed that B1-8 B cells extracted significantly more high-affinity NIP_{10} than low-affinity NP_{10} from both FDCs and DCs (Fig. 6, C and D). Although B cells extracted similar amounts of antigen from both APCs, the ratio of total NIP_{10} to NP_{10} extracted was a mean of fourfold higher on FDCs (Fig. 6 E). Thus, B cells achieve more stringent affinity discrimination during extraction of antigen from immune synapses formed with FDCs than DCs.

It is possible that the efficiency of antigen extraction is regulated by different antigen-presenting receptors on the APCs or by engagement of different adhesion and signaling receptors on the B cells. To further probe the effect of APC physical properties on B cell antigen extraction, we manipulated the stiffness of FDCs using mycalolide B, an irreversible inhibitor of actin polymerization (Saito et al., 1994). Disrupting the actin cytoskeleton results in a stark decrease in cell stiffness (Wakatsuki et al., 2001). B1-8 B cells extracted significantly more NIP_{10} than NP_{10} antigen from both the actin-inhibited and DMSO-treated FDCs (Fig. 6 F), although affinity discrimination

Downloaded from http://rupress.org/jcb/article-pdf/216/1/217/1373975/jcb_201607064.pdf by The Francis Crick Institute user on 20 October 2020

was a mean of 2.5-fold better from the control FDCs compared with those treated with mycalolide B (Fig. 6 G). Interestingly, B cells extracted different components of the immune complex depending on the physical properties of the FDCs. When antigen was tethered via immune complexes to the DMSO-treated FDCs, B cells extracted antigen by rupturing it from the tethering antibody (Fig. 6 H). However, B cells acquired antigen together with the tethering antibody into the same endosomal compartments from the actin-inhibited FDCs, suggesting that differences in APC stiffness cause B cells to internalize different combinations of proteins from immune complexes.

Discussion

Antibody responses require the selection and expansion of high-affinity B cell clones. Selection is achieved through affinity-dependent internalization of antigen from APCs, although the mechanism by which high-affinity antigens are preferentially internalized remains unclear. In the work presented here, we developed new DNA-based nanosensors that allowed the first in situ measurements of B cell antigen extraction from live cell–cell contacts. Importantly, we found that B cells exclusively used mechanical force to extract antigen from live APCs. In addition, mechanical extraction of antigen was regulated by physical properties of the immune synapse, such as the strength of the antigen tether and stiffness of the APC membrane. These properties affected the strength of B cell extraction forces and the requirements for BCR affinity.

Although we conclude that mechanical force is the dominant antigen extraction mechanism, our data do support a role for enzymatic liberation of immobilized antigen. We observed degradation of synaptic antigen when it was tethered strongly to a noninternalizable surface, in agreement with previous studies using antigen covalently coupled to noninternalizable latex beads (Yuseff et al., 2011; Reversat et al., 2015). It is possible that enzymatic degradation plays a role in antigen acquisition from stiff physiological substrates such as bone (Li et al., 2010), cartilage (Ciechomska et al., 2014), or bacterial biofilms (Gil et al., 2014). The fragments of antigen liberated in this process are endocytosed by unknown pathways, but do lead to peptide loading onto MHCII (Yuseff et al., 2011).

However, we observed that mechanical extraction of very small amounts of antigen abolished enzymatic extraction. It appears that B cells first attempted to acquire antigen through physical force and switched to enzymatic degradation if mechanical extraction was unsuccessful. We did not observe B cells using the two mechanisms cooperatively in any of our experiments. In fact, enzymatic degradation is incompatible with mechanical discrimination of antigen affinities (Natkanski et al., 2013). Enzymatic release of antigen from the presenting surface would disrupt the tension across the BCR–antigen bond, which is required to test binding strength and promote affinity-dependent internalization (Tolar and Spillane, 2014).

Although the signaling pathways underlying the switch from enzymatic to mechanical antigen extraction are not yet known, we observed that lysosomes quickly colocalized with endosomes containing mechanically extracted antigen, but were gradually transported to the synapse when physical extraction of antigen failed. It is possible that lysosomes are passively transported to the synapse as the result of B cell polarization (Stinchcombe et al., 2006). Alternatively, lysosome recruitment may actively be driven by Ca^{2+} entering through a disrupted synaptic membrane, which can trigger vesicle–vesicle and vesicle–plasma membrane fusion (Rodríguez et al., 1997; Reddy et al., 2001). The idea that there is a molecular switch regulating mechanisms of B cell antigen extraction is intriguing, and an interesting topic of investigation for future studies.

Our data suggest a rather nuanced relationship between the efficiency of antigen extraction and the physical characteristics of antigen presentation, with flexible substrates promoting more efficient antigen extraction and stiff substrates promoting more stringent affinity discrimination. On a stiff substrate, the pulling exerted by the B cell quickly builds the mechanical load on the BCR–antigen bond and leads to bond failure, whereas the viscoelasticity of a flexible membrane substrate limits the mechanical load (Bangasser et al., 2013). We observed this effect not only on the artificial antigen-presenting substrates, but also on live APCs. Direct measurements of APC membrane stiffness using AFM revealed that FDCs were stiffer substrates than DCs, which resulted in higher forces applied by the B cells as revealed by separation of a DNA-based tension sensor or rupture of antigen from its tethering antibody. Consistent with data from artificial substrates, the stiffer FDCs also promoted better affinity discrimination than the flexible DCs, and this could be inhibited by selective disruption of the FDC actin cytoskeleton.

These findings could have important implications for the regulation of different stages of B cell responses. Naive B cells have been shown to interact with FDCs before the onset of the GC, and affinity discrimination may be important for selection of pre-GC cells into the GC reaction (Schwickert et al., 2011). Although the data presented here were obtained using naive B cells, it can be predicted that the mechanical properties of FDCs play an important role in B cell clonal selection during GC reactions. We have previously shown that GC B cells apply stronger synaptic pulling forces than naive B cells (Nowosad et al., 2016), which, combined with stiff FDCs, would lead to stringent affinity discrimination and promote affinity maturation of antibodies. In contrast, naive B cells extract antigen from DCs using relatively weak pulling forces, resulting in better acquisition of low-affinity antigen. This scenario presumably would allow low-affinity B cell clones to initiate antibody responses when high-affinity clones are not available, and is consistent with the observation that high- and low-affinity B cell clones have similar intrinsic capacity to respond to antigen in vivo (Dal Porto et al., 2002; Shih et al., 2002). Although higher forces and more stringent affinity discrimination on stiff substrates are consistent with the physical characteristics of the actomyosin cytoskeleton pulling over short distances (Jiang et al., 2006), we note that additional regulation may come from stronger BCR signaling observed on stiff substrates (Wan et al., 2013, 2015).

We have demonstrated that different antigen extraction mechanisms, including enzymatic liberation, pinching off soft membranes, and ripping antigen from stiff membranes, cause B cells to acquire different components of complex antigens. In vivo, the effect may be qualitative differences in the resulting peptide MHC repertoire. The requirement for rupturing the immune complex from the FDC is also compatible with the idea that the affinity of the tethering antibody impacts affinity maturation in the GC (Zhang et al., 2013). Further investigation of the mechanical properties of APCs and the cell-surface receptors involved in antigen presentation to B cells may reveal novel mechanisms controlling B cell responses and inform new approaches for vaccine design. If B cell responses can be

Downloaded from http://rupress.org/jcb/article-pdf/216/1/217/1373975/jcb_201607064.pdf by The Francis Crick Institute user on 20 October 2020

tuned through physical cues received in the immune synapse, then manipulating the mechanical properties of particle- or APC-based vaccines (Palucka and Banchereau, 2012; Wen and Collier, 2015) may enhance T-dependent antibody production and affinity maturation.

Materials and methods

Mice

B1-8$^{flox/flox}$ Igκ$^{Ctm1Cgn/tm1Cgn}$ mice on a C57BL/6 background (B1-8 mice) were used as the source of naive B cells specific for the NIP and NP haptens for all experiments unless stated otherwise. C57BL/6 mice were used as the source of FDCs and DCs. All mice were 1–6 mo old, and both males and females were used. Mice were bred and treated in accordance with guidelines set by the UK Home Office and the Francis Crick Institute Ethical Review Panel.

B cell isolation

Primary splenocytes were obtained by passing the spleen through a 70-µm cell strainer and lysing red blood cells using ACK lysis buffer (Gibco). Naive B cells were isolated in MACS buffer (PBS, pH 7.3, 5% BSA, and 1 mM EDTA) using an autoMACS Pro Separator by negative selection with anti-CD43 mouse microbeads (Miltenyi Biotec). B cells were cultured at a density of 5×10^6 cells/ml in full RPMI (RPMI 1640 medium [Sigma-Aldrich] supplemented with 10% FBS [Biosera], 1% MEM nonessential amino acids [Gibco], 2 mM L-glutamine [PAA Laboratories], 50 µM 2-mercaptoethanol [Gibco], 100 U/ml penicillin, and 100 µg/ml streptomycin).

Artificial antigen-presenting substrates

Glass substrates were covalently functionalized with biotin as previously described (Zhang et al., 2014). In brief, glass coverslips (no. 1.5, 24 × 50 mm; VWR International) were etched with piranha solution (2:1 H_2SO_4/H_2O_2) for 15 min, washed 10 times with ultrapure water (Milli-Q; EMD Millipore), and rinsed three times with ethanol (caution: piranha solution is extremely corrosive). The coverslips were placed in a beaker containing 1% (3-(2-aminoethylamino)propyl)trimethoxysilane (Sigma-Aldrich) in ethanol for 45 min. The coverslips were then washed four times with ethanol, dried with argon, baked in an oven at 100°C for 10 min, and allowed to cool to RT. Sample chambers were assembled by placing a 10-µl CultureWell gasket (Grace Bio-Labs) onto the coverslip, which was then glued onto a one-well Nunc Lab-Tek chamber (Thermo Fisher Scientific). The wells were incubated with 2 mg/ml NHS-PEG_4-biotin (Thermo Fisher Scientific) in DMSO overnight at RT, washed with ethanol, dried, and washed with PBS. The wells were incubated sequentially for 20 min with 2% BSA in PBS, 1 µg/ml streptavidin that was labeled with Alexa Fluor 405 NHS ester (AF405; Thermo Fisher Scientific), and 10 nM sensor, resulting typically in a density of 25 DNA sensors/µm^2.

PLBs were prepared by mixing 99% 1,2-dioleoyl-sn-glycero-3-phosphocholine and 1% 1,2-dioleoyl-sn-glycero-3-phosphoethanolamine-*N*-(cap biotinyl) (Avanti Polar Lipids, Inc.) in chloroform. The solvent was dried with a gentle stream of argon and then under vacuum for 1 h. The lipid film was resuspended in degassed PBS to a final concentration of 5 mM and bath sonicated for 2 h to produce small unilamellar vesicles (SUVs). The vesicles were centrifuged for 14 h at 55,000 *g* to yield a clear SUV suspension. Bilayers were prepared by adding 10 µl of 0.2 mM SUV suspension in PBS to a CultureWell gasket attached to a piranha-etched coverslip as described earlier. The wells were incubated sequentially for 20 min with 1 µg/ml streptavidin (unlabeled or labeled with AF405) and 1 µg/ml protein antigen or 10 nM sensor, which equaled a density of ∼70 antigen molecules or DNA sensors/µm^2.

To make PMSs, HEK293T cells were cultured in an eight-well Nunc Lab-Tek chamber coated with poly-L-lysine (Sigma-Aldrich) for 12 h at 37°C with 5% CO_2 in DMEM supplemented with 10% FBS, 1% MEM nonessential amino acids, 2 mM L-glutamine, 100 U/ml penicillin, and 100 µg/ml streptomycin to 100% confluence (200,000 cells per well). Wells were washed with PBS and sonicated with a probe sonicator. The exposed glass was blocked with 1% BSA in PBS for 30 min at RT. PMSs were exchanged into 0.1% BSA in HBSS (BSA/HBSS) and incubated for 20 min sequentially with 1 µg/ml biotinylated annexin V (BioVision), 1 µg/ml streptavidin (unlabeled or labeled with AF405), and 1 µg/ml protein antigen or 10 nM sensor, resulting in an approximate density of 50 antigen molecules or DNA sensors/µm^2.

Immune complex generation

Immune complexes were generated by mixing 0.5 µg biotin Armenian hamster IgG isotope control antibody (BioLegend), 0.375 µg goat anti–hamster (Armenian) IgG antibody (DyLight488 or DyLight649; BioLegend), 10 µl freshly isolated mouse serum (as a source of complement), and 40 µl GVB^{2+} buffer (Complement Technology) for 30 min at 37°C.

FDC isolation, ex vivo culture, and antigen loading

FDC isolation and culture procedures were adapted from those described (El Shikh et al., 2006; Heesters et al., 2013). Lymph nodes (superficial and deep cervical, brachial, axillary, mesenteric, and inguinal) were harvested from four C57BL/6 mice, teased apart using 25G needles, and digested in 2 ml DMEM with 20 mM HEPES, 0.26 U Liberase DH, and 2,000 U DNase I (Roche) for 45 min at 37°C. Released cells were collected and the lymph nodes were digested a second time with fresh reagents. All released cells were pooled, washed in 50 ml DMEM with 10% FBS, and then incubated sequentially with an FDC-specific antibody (FDC-M1, 1.6 µg antibody per 2×10^7 cells; BD) for 1 h, 1 µg biotin mouse anti–rat Ig, κ light chain (clone MRK-1; BD) for 45 min, and with 50 µl antibiotin microbeads (Miltenyi Biotec) for 20 min on ice. The FDCs were isolated by positive selection in MACS buffer using an autoMACS Pro Separator. Positively selected FDCs were resuspended in FDC medium (DMEM supplemented with 10% FBS, 20 mM Hepes, 2 mM L-glutamine, 1 µg/ml gentamicin, and 0.2 mM MEM nonessential amino acids) and plated onto collagen-coated (rat tail–derived collagen; Roche) FluoroDish cell culture dishes (10-mm well; World Precision Instruments) at a density of 4×10^5 FDCs per dish. FDCs were cultured at 37°C with 5% CO_2 and used at day 5–7.

FDCs were exchanged into BSA/HBSS and incubated sequentially with the biotinylated immune complex mix, 1 µg/ml streptavidin, and 1 µg/ml protein antigen (NIP_{10} or NP_{10}) or 10 nM DNA sensor, for 30 min at 4°C. FDCs were washed with BSA/HBSS and warmed to 37°C for 10 min before adding B cells to the imaging well.

Mycalolide B treatment of FDCs

To measure B cell antigen extraction from actin-inhibited FDCs, FDCs were treated with 3 µM mycalolide B for 1 h at 37°C in FDC medium. Excess mycalolide B was removed by washing FDCs with BSA/HBSS before loading antigen as described earlier.

Bone marrow–derived DC isolation, ex vivo culture, and antigen loading

Bone marrow was flushed from two femurs of a C57BL/6 mouse using full RPMI and passed through a 40-µm cell strainer. Cells were plated onto collagen-coated FluoroDish cell culture dishes at a density of 4×10^5 bone marrow–derived dendritic cells per dish in full RPMI containing 20 ng/ml recombinant mouse granulocyte-macrophage colony-stimulating factor (R&D Systems). Cells were cultured at 37°C with 5% CO_2 and used at day 5–7.

Downloaded from http://rupress.org/jcb/article-pdf/216/1/217/1373975/jcb_201607064.pdf by The Francis Crick Institute user on 20 October 2020

Bone marrow–derived dendritic cells were exchanged into BSA/HBSS and incubated sequentially with the biotinylated immune complex mix, 1 µg/ml streptavidin, and 1 µg/ml protein antigen (NIP_{10} or NP_{10}) or 10 nM DNA sensor for 30 min at 4°C. DCs were washed with BSA/HBSS and warmed to 37°C for 10 min before adding B cells to the imaging well.

B cell assays

To measure unquenching of the DNA degradation sensor using flow cytometry, C57BL/6 naive B cells were incubated sequentially on ice with 1 µg/ml goat $F(ab')_2$ anti-mouse Igκ (anti-Igκ; SouthernBiotech) that was biotinylated with sulfo-NHS-LC-LC-biotin (Thermo Fisher Scientific) and labeled with Cy3 monoreactive NHS ester (GE Healthcare), 1 µg/ml streptavidin, and 100 nM of the DNA degradation sensor at 4°C for 20 min. The cells were washed with BSA/HBSS between each incubation step. Half of the cells were then incubated at 37°C for 20 min to allow the B cells to internalize the antigen. Cells were fixed with 2% PFA for 15 min at RT and labeled with 1 µg/ml anti–mouse CD45R/B220 antibody (Brilliant Violet 421; BioLegend) before analysis by flow cytometry.

To measure colocalization of DNA and protein degradation, C57BL/6 naive B cells were incubated for 20 min on ice with 1 µg/ml biotin-AF405 anti-Igκ antigen and tethered via streptavidin to the DNA degradation sensor and biotinylated rabbit polyclonal anti-BSA IgG (Thermo Fisher Scientific) complexed with DQ-BSA (Thermo Fisher Scientific). The cells were incubated at 37°C for 0–20 min, seeded onto glass coated with poly-L-lysine, fixed with 2% PFA for 15 min at RT, and labeled with 1 µg/ml PerCP/Cy5.5 B220 antibody before imaging.

To measure enzymatic degradation in synapses on PLBs or PMSs, PLBs and PMSs were loaded sequentially for 20 min with 1 µg/ml biotin-Cy3 NIP_{10} antigen (goat IgG $F(ab')_2$ fragment [Jackson Immunoresearch Laboratories, Inc.] biotinylated, labeled with Cy3, and haptenated with 4-hydroxy-3-iodo-5-nitrophenylacetic active ester [NIP-Osu; LGC Biosearch Technologies]), 1 µg/ml streptavidin, and 10 nM DNA degradation sensor in BSA/HBSS.

For all fixed time point measurements, B cells were incubated with artificial antigen-presenting substrates in BSA/HBSS for 20 min at 37°C or with FDCs and DCs for 30 min at 37°C, unless indicated otherwise. Cells were then fixed for 15 min at RT with 2% PFA, blocked with 5% normal mouse serum (Jackson ImmunoResearch Laboratories, Inc.) for 30 min at RT, and labeled with 1 µg/ml B220 antibody (Brilliant Violet 421 or PerCP/Cy5.5) for 20 min. Cells were then washed and fixed again.

To monitor time-dependent lysosome recruitment to the synapse, cells were incubated with PLBs or PMSs for the indicated times and then fixed. The antigen used in these measurements was biotin-Cy3 anti-Igκ. The antigen was bound directly to the substrates using streptavidin to provide a very strong tether. After fixation, cells were stained with 1 µg/ml PerCP/Cy5.5 B220 antibody, permeabilized using the FoxP3 fixation/permeabilization kit (eBioscience) on ice for 45 min, washed with permeabilization buffer, and blocked with 5% normal mouse serum for 30 min at RT. Cells were then incubated with 3 µg/ml anti–LAMP-1 antibody (rabbit polyclonal; Abcam) for 30 min at RT, washed with permeabilization buffer, and incubated with anti–rabbit IgG (H+L) $F(ab')_2$ AF488 (Cell Signaling Technology) for 30 min at RT. Cells were washed again, fixed, and washed with BSA/HBSS before imaging.

For assays involving interactions between B cells and antigen-presenting substrates, B cells were added at a density of 6×10^6 cells/ml. To image interactions between B cells and FDCs or DCs, 1.5×10^6 B cells per 4×10^5 cultured FDCs or DCs were used.

DNA sensor design

The upper handles of the DNA mechanism and tension sensors contained a thiol modification for covalent coupling to primary amine groups on the protein antigen. After annealing single-stranded oligonucleotides, the DNA and protein were exchanged into degassed PBS-EDTA (PBS, pH 7.3, and 1 mM EDTA) using a 7-kD molecular mass cutoff desalting column (Zeba; Thermo Fisher Scientific). The sensor thiol group was reduced with 50 mM DTT, and the protein primary amines were activated with a fivefold molar excess of sulfosuccinimidyl 4-(*N*-maleimidomethyl)cyclohexane-1-carboxylate (EMD Millipore) for 30 min at RT. Each was passed twice over a desalting column to remove excess reagents. The DNA and protein solutions were mixed and incubated for 1 h at RT, and the DNA–protein conjugate was readily identified by a shift on a 2% agarose gel (Fig. S5 A). The conjugation efficiency was typically >40%. The conjugate was purified using anion exchange chromatography (Mono Q; GE Healthcare) using a buffer gradient of 25 mM Tris, pH 8.0 at 4°C, and 100–1,000 mM NaCl over 45 column volumes (Fig. S5 B). Conjugate fractions were confirmed by agarose gel electrophoresis (Fig. S5 C). The conjugated sensor was exchanged into 0.1 M sodium carbonate/sodium bicarbonate buffer, pH 9.2 (carbonate buffer), using a desalting column and incubated with a 50-fold molar excess of NIP-Osu for 30 min at RT to haptenate the protein. Unreacted NIP-Osu was removed using a desalting column. For the mechanism sensor, the protein was first incubated with a sixfold excess of Atto550 NHS-ester (Atto-tec) for 30 min at RT before haptenation with NIP. Excess dye was removed with a desalting column, and the number of dyes per protein was two to three as determined by UV-visible spectroscopy. For the monovalent NIP_1 and NP_1 tension sensors, the upper handle was modified with a primary amine instead of a thiol for direct conjugation to NIP-Osu or 4-hydroxy-3-nitrophenylacetic acid active ester (NP-Osu; LGC Biosearch Technologies). Sensors were exchanged into carbonate buffer, incubated with a 20-fold excess of NIP-Osu or NP-Osu for 30 min at RT, and desalted to remove unreacted hapten. Monovalent labeling of the sensors was verified using UV-visible spectroscopy. Sensors were stored at −20°C in single-use aliquots.

The DNA sequences were as follows: degradation sensor Atto-647N biotin ss oligo, 5′-Atto647N-TCCGGCTGCCTCGCTGCC GTCGCCA-biotin-3′; degradation sensor Iowa Black RQ ss oligo, 5′-TGGCGACGGCAGCGAGGCAGCCGGA-Iowa Black RQ-3′; nuclease-resistant degradation sensor Atto647N biotin ss oligo, 5′-Atto647N-mU*mC* mC*mG*mG* mC*mU*mG* mC*mC*mU* mC*mG*mC* mU*mG*mC* mC*mG*mU* mC*mG*mC*mC*mA-biotin-3′; nuclease-resistant degradation sensor Iowa Black RQ ss oligo, 5′-mU*mG*mG* mC*mG*mA*mC*mG*mG*mC*mA*mG-mC*mG*mA* mG*mG*mC*mA*mG*mC*mC*mG*mG*mA-Iowa Black RQ-3′; mechanism sensor thiol ss oligo, 5′-S-S-TCACGACAG GTTCCTTCGCATCGATATTTACTCACAAGCAGTGTGTACA-biotin-3′; mechanism sensor lower handle, 5′-Atto647N-TGTACACAC TGCTTGTGAGTAAAT-3′; mechanism sensor upper handle, 5′-CTC GGTGCATAGAACCTGTCGTGA-3′; weak tension sensor upper handle, 5′-AATGTATCATTGTATCTTATAGCTACGCTTCCTTGGACA GCACT-Atto647N-3′; weak tension sensor lower handle, 5′-biotin-ATTTACTCACAAGCAGTGTGTACAATAAGATACAATGATACATT-Atto550-3′; weak tension sensor upper handle complement, 5′-S-S-AGTGCTGTCCAAGGAAGCGTAGCT-3′; weak tension sensor lower handle complement, 5′-TGTACACACTGCTTGTGAGTAAAT-biotin-3′; strong tension sensor upper handle, 5′-GGCGCGCGGCC GGGCGCCGCAGCTACGCTTCCTTGGACAGCACT-Atto647N-3′; strong tension sensor lower handle, 5′-biotin-ATTTACTCACAAGCA GTGTGTACAGCGGCGCCCGGCCGCGCGCC-Atto550-3′; strong tension sensor upper handle complement, 5′-S-S-AGTGCTGTCCAA

Downloaded from http://rupress.org/jcb/article-pdf/216/1/217/1373975/jcb_201607064.pdf by The Francis Crick Institute user on 20 October 2020

GGAAGCGTAGCT-3′; and strong tension sensor lower handle complement, 5′-TGTACACACTGCTTGTGAGTAAAT-biotin-3′.

For the experiments shown in Fig. 3 (C–E) and Fig. S4, the strong tension sensor upper handle contained a 3′ Atto488 in place of Atto647N, and the strong tension sensor lower handle was unlabeled at the 3′ end.

Imaging

All imaging was performed using an IX81 microscope (Olympus) fitted with a 100×, 1.4-NA oil-immersion objective and a motorized stage with an integrated piezo Z-drive (Applied Scientific Instrumentation). The microscope was controlled through MetaMorph software (Molecular Devices). Epifluorescence illumination was provided by diode lasers centered at the following wavelengths: 405 nm (Changchun New Industries), 488 nm (Coherent), 514 nm (Coherent), and 640 nm (Blue Sky Research). The beams were passed through excitation filters and coupled into a multispectral single-mode optical fiber (Oz Optics) connected to the illumination port of the microscope. The fluorescence was filtered through appropriate emission filters using a filter wheel (Sutter Instrument) and imaged onto an Andor Technology iXon EM-CCD camera.

Image processing

Image analysis was performed in a user-guided pipeline in Matlab, as described previously (Nowosad et al., 2016). In brief, image *z*-stacks from each channel were aligned and cropped to remove poorly illuminated areas at the edges. Images were then background-subtracted and corrected for flat-field and spectral bleedthroughs. Cells were detected in the B220 channel, and 3D cell masks containing cell identification numbers were stored as image stacks for subsequent analysis.

Antigen extraction by each cell was analyzed from the *z*-stack images by bandpass-filtering each image plane and identifying antigen clusters above the synapse using a user-specified global threshold. Local background was subtracted from each identified antigen cluster to correct for antigen fluorescence scattered from the substrate. Extracted antigen percentage was calculated as the sum of pixel intensities of the background-corrected extracted clusters divided by the total antigen fluorescence in each cell mask. Masks containing the extracted antigen clusters were used to quantify fluorescence in other channels.

Side-view reconstruction of cells for display was performed using deconvolution as previously described (Natkanski et al., 2013). Because smooth, unclustered signal is removed during the deconvolution procedure, the antigen-presenting substrates are typically not visible in the images, although internalized antigen clusters are clearly visible. In Fig. 2 C, although the DNA mechanism sensor was tightly clustered in B cell synapses on PLBs, the streptavidin remained homogeneously distributed on the PLB surface. As a result, streptavidin is not visibly colocalized with the mechanism sensor in the image, although it was present.

AFM spectroscopy

AFM measurements were performed using a Nanowizard II AFM (JPK Instruments). Gold-coated Biolever cantilevers (nominal spring constant 30 pN/nm; Olympus) were exposed to UV light for 30 min and used immediately. FDCs and DCs were attached to collagen-coated coverslips and imaged in BSA/HBSS. The tip was brought into contact with the cell surface to allow binding to the membrane through electrostatic interactions and was then retracted with a speed of 2 µm/s. Data were processed using JPK analysis software. Rupture forces and rupture distances were measured from force versus tip-sample separation curves containing single-step ruptures.

Online supplemental material

Fig. S1 shows the quenching efficiency of nine different fluorophore–quencher pairs investigated for the design of the DNA degradation sensor (related to Fig. 1). Fig. S2 shows LAMP-1 colocalization with internalized antigen clusters and concomitant DNA sensor degradation (related to Fig. 1). Fig. S3 shows the effect of fluorescence resonance energy transfer on the Atto647N/Atto550 fluorescence intensity ratios for the mechanism sensor (related to Fig. 2). Fig. S4 shows the localization of the mechanism and tension sensors in B cell synapses (related to Fig. 3). Fig. S5 shows the approach for characterizing and purifying the DNA mechanism and tension sensors.

Acknowledgments

We thank Dessi Malinova for assistance with the flow cytometry measurements and Justin Molloy for assistance with AFM measurements.

This work was supported by the H2020 European Research Council (Consolidator Grant 648228) and the Francis Crick Institute, which receives its core funding from Cancer Research UK, the UK Medical Research Council, and the Wellcome Trust. P. Tolar is also supported by the European Molecular Biology Organization Young Investigator Program.

The authors declare no competing financial interests.

Author contributions: K.M. Spillane designed and performed the experiments and analyzed the data. P. Tolar designed the experiments and wrote the image analysis software. K.M. Spillane and P. Tolar wrote the manuscript.

Submitted: 18 July 2016
Revised: 14 October 2016
Accepted: 17 November 2016

References

Bangasser, B.L., S.S. Rosenfeld, and D.J. Odde. 2013. Determinants of maximal force transmission in a motor-clutch model of cell traction in a compliant microenvironment. *Biophys. J.* 105:581–592. http://dx.doi.org/10.1016/j.bpj.2013.06.027

Batista, F.D., and M.S. Neuberger. 2000. B cells extract and present immobilized antigen: Implications for affinity discrimination. *EMBO J.* 19:513–520. http://dx.doi.org/10.1093/emboj/19.4.513

Batista, F.D., D. Iber, and M.S. Neuberger. 2001. B cells acquire antigen from target cells after synapse formation. *Nature.* 411:489–494. http://dx.doi.org/10.1038/35078099

Bergtold, A., D.D. Desai, A. Gavhane, and R. Clynes. 2005. Cell surface recycling of internalized antigen permits dendritic cell priming of B cells. *Immunity.* 23:503–514. http://dx.doi.org/10.1016/j.immuni.2005.09.013

Carrasco, Y.R., and F.D. Batista. 2007. B cells acquire particulate antigen in a macrophage-rich area at the boundary between the follicle and the subcapsular sinus of the lymph node. *Immunity.* 27:160–171. http://dx.doi.org/10.1016/j.immuni.2007.06.007

Castellana, E.T., and P.S. Cremer. 2006. Solid supported lipid bilayers: From biophysical studies to sensor design. *Surf. Sci. Rep.* 61:429–444. http://dx.doi.org/10.1016/j.surfrep.2006.06.001

Ciechomska, M., C.L. Wilson, A. Floudas, W. Hui, A.D. Rowan, W. van Eden, J.H. Robinson, and A.M. Knight. 2014. Antigen-specific B lymphocytes acquire proteoglycan aggrecan from cartilage extracellular matrix resulting in antigen presentation and $CD4^+$ T-cell activation. *Immunology.* 141:70–78. http://dx.doi.org/10.1111/imm.12169

Dal Porto, J.M., A.M. Haberman, G. Kelsoe, and M.J. Shlomchik. 2002. Very low affinity B cells form germinal centers, become memory B cells, and participate in secondary immune responses when higher affinity competition is reduced. *J. Exp. Med.* 195:1215–1221. http://dx.doi.org/10.1084/jem.20011550

Downloaded from http://rupress.org/jcb/article-pdf/216/1/217/1373975/jcb_201607064.pdf by The Francis Crick Institute user on 20 October 2020

El Shikh, M.E., R. El Sayed, A.K. Szakal, and J.G. Tew. 2006. Follicular dendritic cell (FDC)-FcγRIIB engagement via immune complexes induces the activated FDC phenotype associated with secondary follicle development. *Eur. J. Immunol.* 36:2715–2724. http://dx.doi.org/10.1002/eji.200636122

Evans, E.A., and D.A. Calderwood. 2007. Forces and bond dynamics in cell adhesion. *Science.* 316:1148–1153. http://dx.doi.org/10.1126/science.1137592

Fang, Y., C. Xu, Y.-X. Fu, V.M. Holers, and H. Molina. 1998. Expression of complement receptors 1 and 2 on follicular dendritic cells is necessary for the generation of a strong antigen-specific IgG response. *J. Immunol.* 160:5273–5279.

Fleire, S.J., J.P. Goldman, Y.R. Carrasco, M. Weber, D. Bray, and F.D. Batista. 2006. B cell ligand discrimination through a spreading and contraction response. *Science.* 312:738–741. http://dx.doi.org/10.1126/science.1123940

Gil, C., C. Solano, S. Burgui, C. Latasa, B. García, A. Toledo-Arana, I. Lasa, and J. Valle. 2014. Biofilm matrix exoproteins induce a protective immune response against *Staphylococcus aureus* biofilm infection. *Infect. Immun.* 82:1017–1029. http://dx.doi.org/10.1128/IAI.01419-13

Gonzalez, S.F., V. Lukacs-Kornek, M.P. Kuligowski, L.A. Pitcher, S.E. Degn, Y.-A. Kim, M.J. Cloninger, L. Martinez-Pomares, S. Gordon, S.J. Turley, and M.C. Carroll. 2010. Capture of influenza by medullary dendritic cells via SIGN-R1 is essential for humoral immunity in draining lymph nodes. *Nat. Immunol.* 11:427–434. http://dx.doi.org/10.1038/ni.1856

Heesters, B.A., P. Chatterjee, Y.-A. Kim, S.F. Gonzalez, M.P. Kuligowski, T. Kirchhausen, and M.C. Carroll. 2013. Endocytosis and recycling of immune complexes by follicular dendritic cells enhances B cell antigen binding and activation. *Immunity.* 38:1164–1175. http://dx.doi.org/10.1016/j.immuni.2013.02.023

Jiang, G., A.H. Huang, Y. Cai, M. Tanase, and M.P. Sheetz. 2006. Rigidity sensing at the leading edge through $\alpha_v\beta_3$ integrins and RPTPα. *Biophys. J.* 90:1804–1809. http://dx.doi.org/10.1529/biophysj.105.072462

Junt, T., E.A. Moseman, M. Iannacone, S. Massberg, P.A. Lang, M. Boes, K. Fink, S.E. Henrickson, D.M. Shayakhmetov, N.C. Di Paolo, et al. 2007. Subcapsular sinus macrophages in lymph nodes clear lymph-borne viruses and present them to antiviral B cells. *Nature.* 450:110–114. http://dx.doi.org/10.1038/nature06287

Krautbauer, R., M. Rief, and H.E. Gaub. 2003. Unzipping DNA oligomers. *Nano Lett.* 3:493–496. http://dx.doi.org/10.1021/nl034049p

Li, H., S. Hong, J. Qian, Y. Zheng, J. Yang, and Q. Yi. 2010. Cross talk between the bone and immune systems: Osteoclasts function as antigen-presenting cells and activate $CD4^+$ and $CD8^+$ T cells. *Blood.* 116:210–217. http://dx.doi.org/10.1182/blood-2009-11-255026

Lipowsky, R., and U. Seifert. 1991. Adhesion of vesicles and membranes. *Mol. Cryst. Liq. Cryst. (Phila. Pa.).* 202:17–25. http://dx.doi.org/10.1080/00268949108035656

Müller, D.J., J. Helenius, D. Alsteens, and Y.F. Dufrêne. 2009. Force probing surfaces of living cells to molecular resolution. *Nat. Chem. Biol.* 5:383–390. http://dx.doi.org/10.1038/nchembio.181

Natkanski, E., W.-Y. Lee, B. Mistry, A. Casal, J.E. Molloy, and P. Tolar. 2013. B cells use mechanical energy to discriminate antigen affinities. *Science.* 340:1587–1590. http://dx.doi.org/10.1126/science.1237572

Nowosad, C.R., K.M. Spillane, and P. Tolar. 2016. Germinal center B cells recognize antigen through a specialized immune synapse architecture. *Nat. Immunol.* 17:870–877. http://dx.doi.org/10.1038/ni.3458

Palucka, K., and J. Banchereau. 2012. Cancer immunotherapy via dendritic cells. *Nat. Rev. Cancer.* 12:265–277. http://dx.doi.org/10.1038/nrc3258

Phan, T.G., I. Grigorova, T. Okada, and J.G. Cyster. 2007. Subcapsular encounter and complement-dependent transport of immune complexes by lymph node B cells. *Nat. Immunol.* 8:992–1000. http://dx.doi.org/10.1038/ni1494

Qi, H., J.G. Egen, A.Y.C. Huang, and R.N. Germain. 2006. Extrafollicular activation of lymph node B cells by antigen-bearing dendritic cells. *Science.* 312:1672–1676. http://dx.doi.org/10.1126/science.1125703

Reddy, A., E.V. Caler, and N.W. Andrews. 2001. Plasma membrane repair is mediated by Ca^{2+}-regulated exocytosis of lysosomes. *Cell.* 106:157–169. http://dx.doi.org/10.1016/S0092-8674(01)00421-4

Reversat, A., M.-I. Yuseff, D. Lankar, O. Malbec, D. Obino, M. Maurin, N.V.G. Penmatcha, A. Amoroso, L. Sengmanivong, G.G. Gundersen, et al. 2015. Polarity protein Par3 controls B-cell receptor dynamics and antigen extraction at the immune synapse. *Mol. Biol. Cell.* 26:1273–1285. http://dx.doi.org/10.1091/mbc.E14-09-1373

Rodríguez, A., P. Webster, J. Ortego, and N.W. Andrews. 1997. Lysosomes behave as Ca^{2+}-regulated exocytic vesicles in fibroblasts and epithelial cells. *J. Cell Biol.* 137:93–104. http://dx.doi.org/10.1083/jcb.137.1.93

Saito, S., S. Watabe, H. Ozaki, N. Fusetani, and H. Karaki. 1994. Mycalolide B, a novel actin depolymerizing agent. *J. Biol. Chem.* 269:29710–29714.

Schwickert, T.A., G.D. Victora, D.R. Fooksman, A.O. Kamphorst, M.R. Mugnier, A.D. Gitlin, M.L. Dustin, and M.C. Nussenzweig. 2011. A dynamic T cell-limited checkpoint regulates affinity-dependent B cell entry into the germinal center. *J. Exp. Med.* 208:1243–1252. http://dx.doi.org/10.1084/jem.20102477

Shih, T.-A.Y., E. Meffre, M. Roederer, and M.C. Nussenzweig. 2002. Role of BCR affinity in T cell dependent antibody responses *in vivo*. *Nat. Immunol.* 3:570–575. http://dx.doi.org/10.1038/ni803

Stinchcombe, J.C., E. Majorovits, G. Bossi, S. Fuller, and G.M. Griffiths. 2006. Centrosome polarization delivers secretory granules to the immunological synapse. *Nature.* 443:462–465. http://dx.doi.org/10.1038/nature05071

Suzuki, K., I. Grigorova, T.G. Phan, L.M. Kelly, and J.G. Cyster. 2009. Visualizing B cell capture of cognate antigen from follicular dendritic cells. *J. Exp. Med.* 206:1485–1493. http://dx.doi.org/10.1084/jem.20090209

Tolar, P., and K.M. Spillane. 2014. Force generation in B-cell synapses: Mechanisms coupling B-cell receptor binding to antigen internalization and affinity discrimination. *Adv. Immunol.* 123:69–100. http://dx.doi.org/10.1016/B978-0-12-800266-7.00002-9

Victora, G.D., and M.C. Nussenzweig. 2012. Germinal centers. *Annu. Rev. Immunol.* 30:429–457. http://dx.doi.org/10.1146/annurev-immunol-020711-075032

Victora, G.D., T.A. Schwickert, D.R. Fooksman, A.O. Kamphorst, M. Meyer-Hermann, M.L. Dustin, and M.C. Nussenzweig. 2010. Germinal center dynamics revealed by multiphoton microscopy with a photoactivatable fluorescent reporter. *Cell.* 143:592–605. http://dx.doi.org/10.1016/j.cell.2010.10.032

Wakatsuki, T., B. Schwab, N.C. Thompson, and E.L. Elson. 2001. Effects of cytochalasin D and latrunculin B on mechanical properties of cells. *J. Cell Sci.* 114:1025–1036.

Wan, Z., S. Zhang, Y. Fan, K. Liu, F. Du, A.M. Davey, H. Zhang, W. Han, C. Xiong, and W. Liu. 2013. B cell activation is regulated by the stiffness properties of the substrate presenting the antigens. *J. Immunol.* 190:4661–4675. http://dx.doi.org/10.4049/jimmunol.1202976

Wan, Z., X. Chen, H. Chen, Q. Ji, Y. Chen, J. Wang, Y. Cao, F. Wang, J. Lou, Z. Tang, and W. Liu. 2015. The activation of IgM- or isotype-switched IgG- and IgE-BCR exhibits distinct mechanical force sensitivity and threshold. *eLife.* 4:e06925. http://dx.doi.org/10.7554/eLife.06925

Wang, X., and T. Ha. 2013. Defining single molecular forces required to activate integrin and notch signaling. *Science.* 340:991–994. http://dx.doi.org/10.1126/science.1231041

Wen, Y., and J.H. Collier. 2015. Supramolecular peptide vaccines: Tuning adaptive immunity. *Curr. Opin. Immunol.* 35:73–79. http://dx.doi.org/10.1016/j.coi.2015.06.007

Yuseff, M.-I., A. Reversat, D. Lankar, J. Diaz, I. Fanget, P. Pierobon, V. Randrian, N. Larochette, F. Vascotto, C. Desdouets, et al. 2011. Polarized secretion of lysosomes at the B cell synapse couples antigen extraction to processing and presentation. *Immunity.* 35:361–374. http://dx.doi.org/10.1016/j.immuni.2011.07.008

Zhang, Y., M. Meyer-Hermann, L.A. George, M.T. Figge, M. Khan, M. Goodall, S.P. Young, A. Reynolds, F. Falciani, A. Waisman, et al. 2013. Germinal center B cells govern their own fate via antibody feedback. *J. Exp. Med.* 210:457–464. http://dx.doi.org/10.1084/jem.20120150

Zhang, Y., C. Ge, C. Zhu, and K. Salaita. 2014. DNA-based digital tension probes reveal integrin forces during early cell adhesion. *Nat. Commun.* 5:5167. http://dx.doi.org/10.1038/ncomms6167

Downloaded from http://rupress.org/jcb/article-pdf/216/1/217/1373975/jcb_201607064.pdf by The Francis Crick Institute user on 20 October 2020